SIMULATION OF AAM AIRCRAFT OPERATIONS IN URBAN TURBULENT AIRWAKE ENVIRONMENTS

Jan Goericke
Advanced Rotorcraft Technology
Fremont, CA, USA

Marilyn J. Smith
Georgia Institute of Technology
Atlanta, GA, USA

Dooyong Lee
Advanced Rotorcraft Technology
Fremont, CA, USA

ABSTRACT

While designs of Advanced Air Mobility (AAM) and Uncrewed Aerial Vehicles (UAV) have made significant progress, simulation and analysis of the concepts of operation are necessary before these vehicles are deployed for general use. A major area of concern is the safety of flight at comparably low altitudes within urban and suburban areas, where the aircraft operate near the urban infrastructure and in an ambient environment that is significantly different than higher altitudes. A new approach to incorporate these highly unsteady flight conditions into an industry-standard, comprehensive modeling and simulation code, FLIGHTLAB, is proposed and evaluated. The comprehensive model captures the pertinent operational and flight characteristics of an AAM configuration including details addressing the tightly coupled flight and propulsion systems as well as elastic aircraft structures. The methodology has a myriad applications; in this study the impact of turbulence on passenger ride quality is examined and these initial studies indicate that inclusion of the turbulent wake in the urban environment simulations is necessary.

INTRODUCTION

The operation of advanced air mobility (AAM) aircraft in support of urban air mobility (UAM) introduces a new mode of transportation in congested cities by connecting city centers with airports and commercial centers. AAM aircraft currently under development commonly utilize distributed (hybrid-) electric propulsion, lift and thrust propellers, and accommodate up to five passengers. These novel vehicle concepts include smaller vehicles designed for transport of a single passenger, cargo or medical supplies, or observation sensors. A key design requirement is the capability of the aircraft to operate in the urban environment.

The current focus in the community with respect to operational challenges focuses on vortex ring state and downwash/outwash with few extant publications on the challenges the urban operations pose in terms of the ride quality of paying customers, medical ambulances, sensors, or fragile cargo. Simulation of the operation of AAM aircraft in the urban environment promises to increase safety, ride quality, and influence aircraft design.

An analysis focusing on an industry-standard simulation framework coupled with an urban turbulent airwake prediction is applied to the virtual air vehicle. The environmental model provides realistic atmospheric conditions by adding stochastic turbulence to the known steady characteristics of obstacle wakes, interpolating the wind speed with height within a realistic boundary layer. The analysis shows the effect of the flight path and wind conditions on the ride experience of the passengers being transported by the aircraft. AAM operational simulation can utilize established tools and methods for geometrically constrained aspects such as shipboard/rooftop landing, aircraft-ground interactions, etc. New methodologies for modeling and simulation are needed to enable extended flights between urban/suburban vertiports and within the turbulent environment.

The comprehensive flight dynamics model in the UAM flight operations simulation and analysis includes important aspects and characteristics of AAM configurations such as high automation of the flight control system, the tightly integrated flight and electric propulsion systems, and, as proposed in this study, selected aircraft elastic structures and human passenger models.

AAM FLIGHT WITHIN THE ATMOSPHERIC BOUNDARY LAYER

An AAM vehicle is designed to fly lower than traditional rotorcraft within terminal areas that are located in urban or suburban neighborhoods. AAM vehicle flight paths are likely to be within the lower portion of the Earth's atmospheric boundary layer (ABL), which can be very unsteady, as illustrated

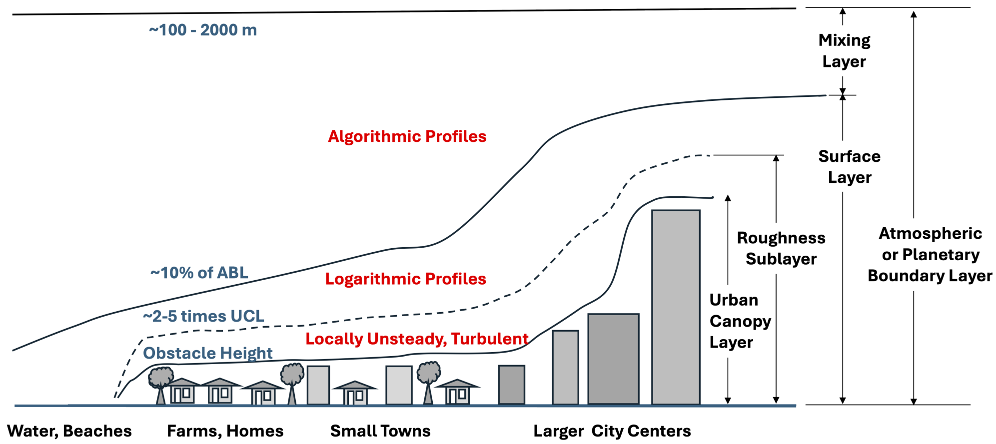

Figure 1: Vertical Structure and Scale of the ABL in an Urban/Suburban Environment (Ref. 1)

in Fig. 1. The wind variation at different altitudes is highly dependent on the local character of the ABL, and flight in the urban boundary layer (UBL) where obstacles contribute additional unsteady components to the steady wind and air turbulence (AT) will be the norm. It is important to understand and include these variations for a myriad of relevant AAM operational use cases, including, but not limited to development of flight plans and the design of vertiports, ensuring passenger comfort, computing vehicle lifecycle costs, and safety assessments.

The microscale portion of the ABL is comprised of the roughness sublayer (RSL) and urban canopy layer (UCL), which vary with location. The effect of highly unsteady features introduced by individual buildings and other obstacles within the urban canopy layer (UCL), along with the roughness sublayer (RSL) where these unsteady, individual features mix prior to becoming more homogeneous at higher altitudes must be computed by more complex methods and models.

In addition to variations due to the local terrain, the ABL (and UBL) will vary diurnally over each 24-hour daily cycle, as well as seasonally. These variations will change the character of the ABL (stable, unstable) which in turn influences how the steady wind velocities change with altitude. Further details of the ABL character can be found in many resources, including Refs. 2–5.

REM: TURBULENT AIRWAKE GENERATION IN THE ROUGHNESS SUBLAYER

To address these local, highly unsteady flowfields, an environmental model is being developed that combines the local or historical weather (temperature, steady wind) with local terrain through user defined or Geographic Information Systems (GIS) to generate accurate representations of the flight environment. This Representative Environment Module (REM) provides a physics-based estimation of the environment with a stochastic or synthetic estimate of the air turbulence (AT). The AT is stochastic and the model will generate varying representations of the turbulence at each use, similar to the atmospheric physics. As the vehicle flies through the GIS- or user-developed flight route, the changing velocities are generated by REM and applied to the flight model, in this case, FLIGHTLAB.

The model applies wake wind transients around buildings by applying reduced-order models of nominal canonical shapes developed through machine learning from a design of experiments using the Lattice-Boltzmann Method (LBM). The machine learning model provides the ability to extend the unsteady wake information from a baseline building shape to multiple shapes and wind orientations. A baseline version of the REM was demonstrated with a simple linear model in Waanders et al. (Ref. 1). An improved nonlinear machine learning model that more accurately and efficiently replicates the unsteady turbulent magnitudes and frequencies is presented in Seeyave and Smith (Ref. 6). This model, comparable to the LBM data, will be integrated into the REM in August 2025. To ensure accurate assessments of the ride quality, LBM training data applied as a surrogate to the REM, were integrated into the FLIGHTLAB simulations for the results herein. Evaluations of the LBM data with new REM data indicate that they are very similar; the reader is referred to Ref. (Ref. 6).

REM Validation

The REM has been validated with LBM, a limited number of high-fidelity wall-modeled large eddy simulations (WMLES) and experimental data (Ref. 1). An example of the REM airwake predictions at designated locations behind a nominal building are compared with LBM simulations at a flight-altitude steady wind speed of 5 m/s, as illustrated in Fig. 2. Additional stochastic turbulence drives these predicted velocities to be higher or lower and adds additional turbulence intensity (unsteadiness) to the predictive winds.

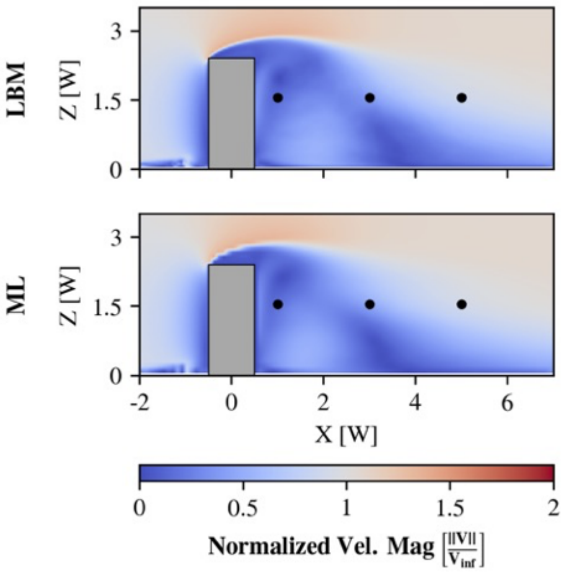

a) LBM and the REM (ML) flowfields

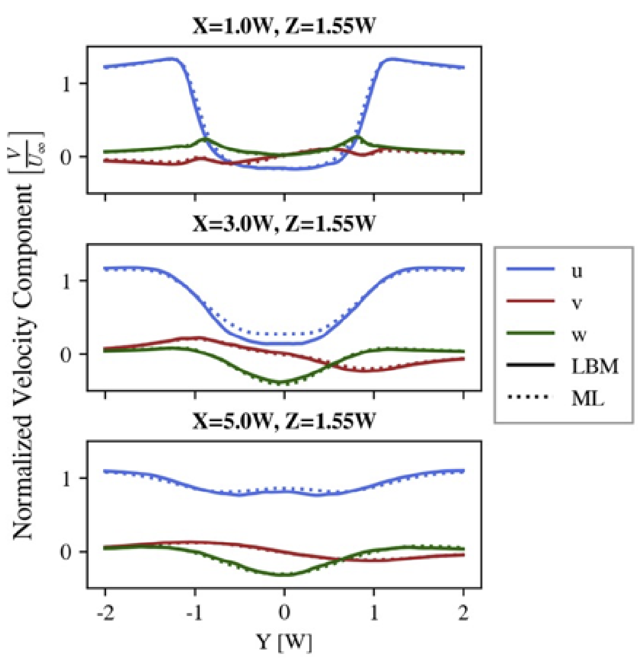

b) Winds encountered at different flight locations

Figure 2: Comparison of the flowfields predicted by the REM (ML) around a 120 m H x 50 m D x 50 m W building for a uniform inflow of 10 m/s at the flight altitude (Ref. 1)

COMPREHENSIVE MODELING AND SIMULATION OF AAM CONFIGURATIONS

In continuation of studies in Refs. 7–9 the FLIGHTLAB comprehensive simulation model of the NASA lift-plus-cruise configuration (Refs. 10, 11), was expanded and enhanced for the simulation of AAM aircraft operations in urban turbulent airwake environments and with the objective to support multiple engineering disciplines in the design and development of these aircraft. The main components of the comprehensive simulation model include the flight dynamics model, flight controller with autopilot functionality, the UAM airwake model, a physics-based electric propulsion system, and a newly developed human passenger model.

Flight Dynamics Model

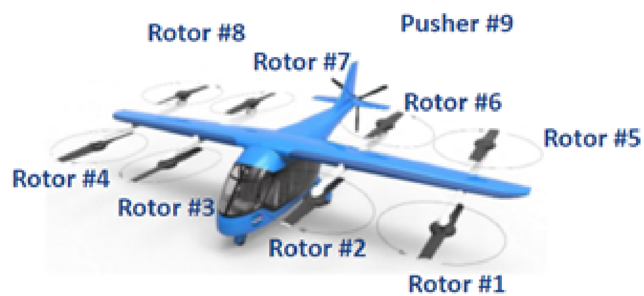

Figure 3: Lift-Plus-Cruise AAM Configuration from Ref. 10, 11

The FLIGHTLAB flight dynamics model (FDM) of the NASA lift-plus-cruise AAM configuration from Ref. 7 and shown in Fig. 3 was used as a starting point. The model was enhanced including an expanded UAM airwake model, tuned autopilot functionality, added heat dissipation model for the electric propulsion system, and the development and integration of a human passenger model.

The configuration consists of eight rigid-blade lift rotors mounted to fore and aft pylons off the wing box. The lift rotors were two-bladed, with a radius of 1.52 m (5 ft), and approximately 10° of linear blade twist. The blade airfoil was approximated using aerodynamic coefficients as a function of angle of attack and Mach number for the SC1095 airfoil. An unsteady airloads model and 30 aerodynamic segments were used for the blade airloads. The rotor/propeller inflow and wake were modeled with the Peters-He finite state model (Ref. 12). The three-bladed pusher propeller with a radius of approximately 1.37 m (4.5 ft) was modeled similarly to the lift rotors. The lift rotor and pusher propeller models in this study were constant-speed with variable collective blade pitch-control for both simplicity and to avoid the potentially significant time delays associated with variable rotor speed control. The lift rotors were canted approx. 8° about the longitudinal axis for aircraft yaw control. The lift rotors and pusher propeller were operating at rotational speeds of 907 and 1,050 rpm, respectively. The rigid main wing with an approximately 14.6 m (48 ft) wingspan was comprised of a notional general aviation airfoil. The total vehicle weight was 2631 kg (5,800 lbs). The configuration included a fuselage airloads model with notional aerodynamic coefficients as a table look-up. The equivalent flat plate drag budget for the fuselage was set at 0.155 m^2 (1.67 ft^2). The vertical and horizontal tail surfaces were modeled as two-dimensional aerodynamic surfaces using aerodynamic coefficients of a symmetrical airfoil. FDM variants with ideal engine (i.e., no drivetrain dynamics) and detailed electric propulsion models supported the investigations in this study.

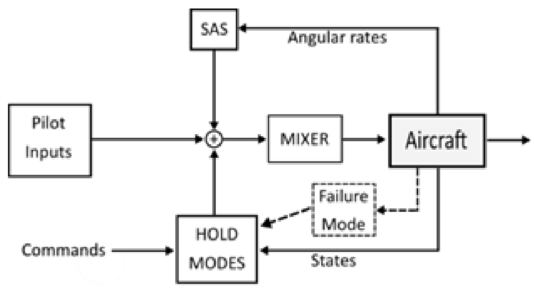

Figure 4: Flight Control System Schematics

Flight Control System The architecture of the flight control system (FCS) used in this study and the integration with the electric propulsion system is illustrated in Fig. 4. The flight control model consists of classical pilot stick controls, i.e., longitudinal, lateral, collective, and pedal, a stability augmentation system (SAS), and a hold modes controller which provides flight control inputs to follow a desired trajectory command. The flight control mixer for the lift-plus-cruise AAM configuration distributed the control inputs to the lift rotors and the pusher propeller. Aircraft pitch control was provided by differential thrust of the fore and aft lift rotors, lateral control by left/right differential thrust, and yaw control by a combination of differential torque and thrust of the canted lift propellers. A pusher propeller aft of the horizontal stabilizer provided forward thrust via a power level control input. Lift rotors and pusher propeller thrusts were controlled by variations of the blade collective pitch while maintaining a constant rotational speed.

Stability augmentation systems play a crucial role in enhancing the stability and control of various vehicles, particularly rotorcraft. The hold modes controller had two major modes in the longitudinal and lateral channels, a velocity hold mode and a position hold mode. Both modes used "desired" velocity commands as inputs. While the velocity hold mode used the velocity command directly as the desired velocity, the position error was converted to desired velocities in the position hold mode. The architecture and functionality of the flight control system was maintained from Ref. 7. The hold mode gains were tuned based on the experience in the previous study and to follow more closely the desired flight path in the presence of the turbulent urban airwake.

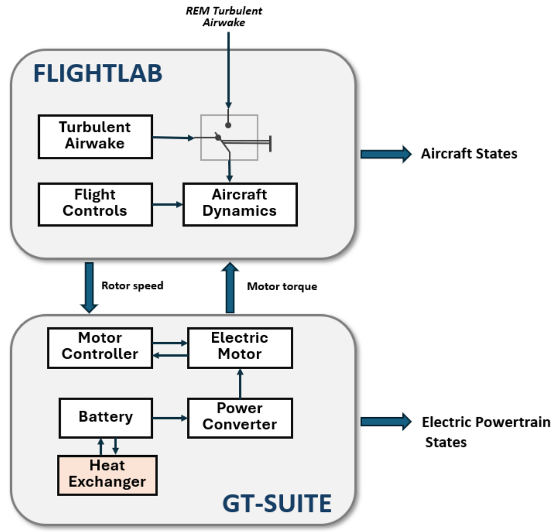

Figure 5: FCS/Propulsion System Integration

Electric Propulsion System Model Previous work in Ref. 7 leveraging the GT-SUITE (Ref. 13) comprehensive set of libraries and components for the modeling of the electric propulsion system, the GT-SUITE and FLIGHTLAB co-simulation was included in this study for providing representative interactions between the rotorcraft flight dynamics and the electric powertrain components, see Fig. 5. The electric propulsion system has individual motor controllers maintaining constant motor speeds as the motor torque demands vary due to control of rotor thrusts through collective blade pitch-control by the FCS.

The thermal system modeling of powertrain components is essential to predict component temperatures to understand potential thermal failures (e.g., thermal runaway in battery packs) and to analyze the impact of component temperatures on performance during transient flight maneuvers. The weight of the thermal control components is also an important consideration for aircraft design and was therefore expanded in this study. Detailed three-dimensional (3D) thermal models can be simulated in GT-SUITE, but are are generally unsuitable for integration into comprehensive system models due to the computationally intensive nature. Therefore, simplified one-dimensional (1D) lumped thermal mass models are typically used to represent the thermal behavior of electric powertrain components, including electric motors, inverters, batteries, and heat exchangers. The computationally efficient 1D thermal models allow for the calculation of temperatures across various sub-components and enable feedback of temperature data into the physics-based models of batteries, inverters, and electric motors affecting the flight dynamics and performance.

Battery Cooling: GT-SUITE provides a framework for modeling thermal management systems with relative ease. For this study, an air-to-water heat exchanger was integrated into the coupled FLIGHTLAB–GT-SUITE simulation environment, see Fig. 5, to provide thermal regulation for the battery pack during AAM operation. The heat exchanger features a finned tube design, which increases the surface area available for heat transfer, thereby maximizing the thermal exchange between the working fluid and ambient air. A schematic of the heat exchanger is depicted in Fig. 6.

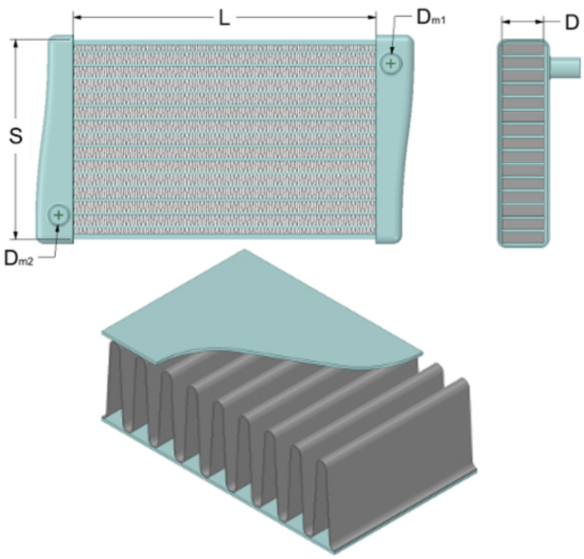

Figure 6: Heat Exchanger Model

The heat exchanger model is defined through its geometric parameters, heat transfer characteristics, and fluid flow properties. It is thermally connected to the battery pack via a pipe system. Heat transfer from the battery to the coolant is modeled through both conductive and convective mechanisms using an intermediate cooling plate, which transfers the thermal load to the water circulating in the cooling loop. To assess the performance of the cooling system, a series of simulations were conducted using a one-minute hover-hold maneuver.

Figure 7 illustrates the battery temperature evolution during this maneuver. In the absence of cooling, the high current demand causes the battery temperature to rapidly rise to approximately 390 K. To mitigate this, two heat exchanger configurations of different sizes were modeled, while keeping material selection and overall cooling circuit design constant. The larger heat exchanger, dimensions: 468 × 639 × 33 mm, was capable of stabilizing the battery temperature around 335 K. In comparison, the smaller heat exchanger, dimensions: 950 × 1002 × 57 mm, maintained a steady-state battery temperature of approximately 340 K. By specifying both the material properties and geometric details of the heat exchangers, a mass estimation was also performed. The total core dry mass of the smaller heat exchanger is approximately 2 kg (4.4 lb), whereas the larger version has a dry mass of 6 kg (13.2 lb).

Turbulent Airwake Data Integration The ride comfort simulation for the *hover-hold* and *approach to hover* maneuvers applied the airwake data and model integration as described in Ref. 7, see also Fig. 8. Since the flight geometric domain was limited to the operation around a rooftop landing spot, the comprehensive simulation model of the NASA lift-plus-cruise configuration used the ship airwake template available in the FLIGHTLAB software application. This

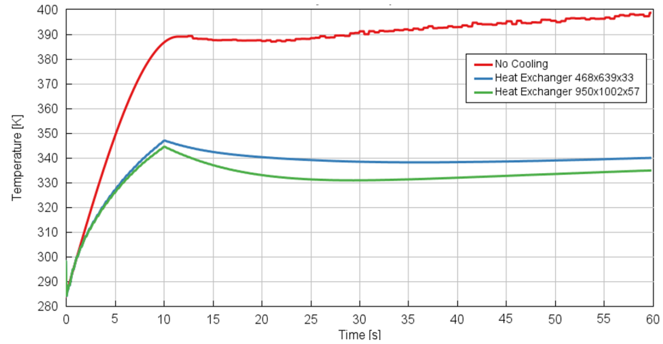

Figure 7: Battery Pack Temperature with Heat Exchanger Model

FLIGHTLAB template permits inclusion of multidimensional full-field wake turbulence data from any source for various applications, including urban and ship airwakes.

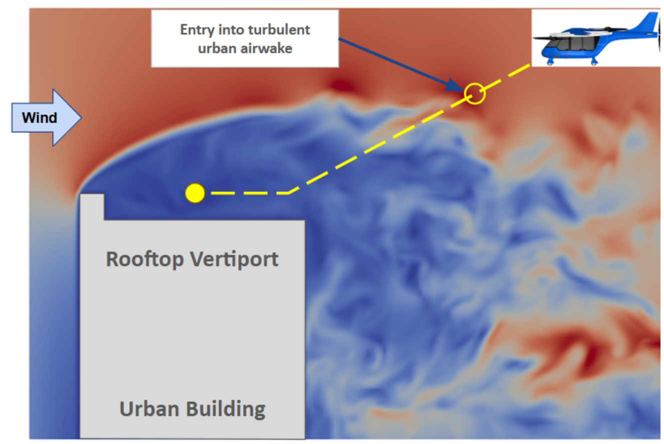

Figure 8: AAM Aircraft Approach Trajectory to Rooftop Landing Spot. Normalized velocities range from -1 (blue) to 1 (red), with deeper colors extending beyond the normalized range.

For the ride comfort simulation of the *straight and level flight* through the city canyon, the airwake data from the REM or real-time LBM approaches will be available in FLIGHTLAB as part of an on-demand process which provides the local velocity components of any model aerodynamic computation point (ACP) with respect to the ACP location within the UAM airwake domain, see also illustration in Fig. 5. This external process helps with reducing the computational effort in the flight dynamics model as the turbulent airwake information is provided to the model and directly applied to the ACPs, for which this study serves as a proof of concept. The external process pre-calculated the time histories of the UAM airwake for a single aircraft ACP, e.g., at the center of gravity of the aircraft, and the flight trajectory. The time histories of the ambient wind x, y, z components were directly applied to all aircraft ACPs for the ride comfort simulation discussed in this paper. Although this is a simplification, it exercises the envisioned implementation for this new process of coupling FLIGHTLAB with an external airwake data generating software process.

Elastic Fuselage Model Elastic structural properties are often not available or sufficiently mature early in aircraft design. However, to explore the effect of elastic structures on the ride quality predictions, a flight dynamics model with elastic fuselage was developed to allow for a comparison between the rigid-body flight dynamics model and a model with elastic fuselage. Tamer et al. (Ref. 14) also considered elastic structures. The FLIGHTLAB elastic fuselage dynamic model includes both rigid body 6 degrees of freedom (DOFs) and elastic motion of the fuselage. The elastic body is connected through a set of predefined elastic joints that passes the elastic motion and transmits loads to the subsystems (rotors, wings, etc.) concerned. The elastic body motion is modeled using the modal body component. The modal data for the elastic body were notional for this study and included preliminary information of elastic fuselage modal frequency, modal damping, and mode shapes. Elastic joints for each lift rotor were added. The notional modal data used excluded rigid body DOFs.

Human Passenger Model

The biodynamic passenger model in Ref. 14 consisted of a series of point mass, spring, and damper elements and was based on a modified Wan-Schimmels (Ref. 15) model for the human body, and a Choi-Wereley (Ref. 16) representative seat and cushion. The biodynamic model was originally developed to simulate the ride comfort of truck operators to reduce the discomfort and long-term health risks. The approach involved developing a simple, linear, 4-DOF lumped parameter model of a seated human to simulate dynamic response to vertical vibration. The model was expanded to include a 2-DOF seat suspension model (Ref. 16). The biodynamic passenger model was employed to study and and evaluate several standards for assessing human sensitivity to vertical vibration. It utilizes a constrained optimization program to determine seat suspension parameters that minimize these standards. While the model was simple and geared toward seat optimization for truck drivers, it was previously applied to estimate the human sensitivity to vertical vibration as experienced by occupants of eVTOLs operating in the turbulent urban environment in Tamer et al. (Ref. 14).

Figure 9a) illustrates the human passenger model. The human body is modeled as a series of spring and damper elements with mass elements for the head m_4, shoulders m_3, stomach m_2, hips m_1, and seat m_s, resulting in four translational degrees of freedom in the model. The stomach mass is parallel to the torso, i.e., connection between hip and shoulders. The passenger model is sensitive to accelerations in the vertical direction from the seat, z, as this is the dominant direction where truck driver discomfort was reported. The current study assumes that this also holds true for AAM aircraft crew and passengers.

Figure 9b) illustrates the human passenger biodynamic model as a new option implemented in FLIGHTLAB. The degrees of freedom are arranged such that all originate from the structural attachment point of the seat to the cabin floor, *GROUND*,

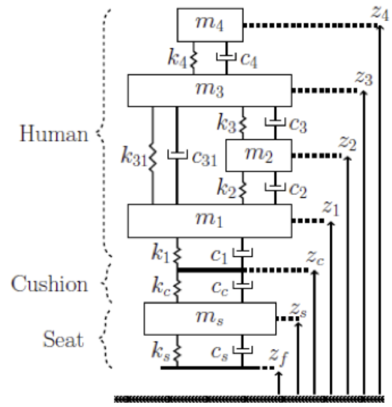

a) Human Passenger Biodynamic Model (Ref. 14)

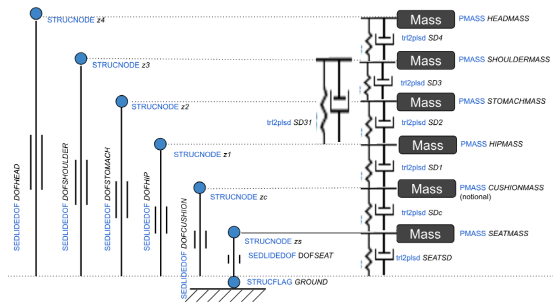

b) Passenger Model in FLIGHTLAB

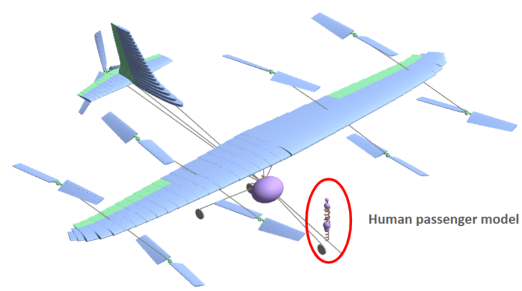

c) Lift-Plus-Cruise AAM with Human Passenger Model

Figure 9: Human Passenger Biodynamic Model

of the aircraft model. Three rotate components were implemented to permit specification of the orientation of the passenger using the three Euler angles and with respect to the aircraft attachment point. Thus, the passenger model can be placed anywhere on the aircraft in the desired orientation.

An additional modification was applied to the human passenger model proposed in Ref. 14. The passenger weight can be adjusted for usage of both standard (Ref. 17) and customized passenger weights. The scaling of point masses for the human body based on total weight is an acceptable approximation based on Ref. 18.

Figure 9c) presents the engineering rendering of the flight dynamics from the FLIGHTLAB model viewer. The human passenger model is annotated in the image. The passenger is located at the approximate location of the pilot seat position in the notional NASA lift-plus-cruise AAM configuration used as an example for this study.

The frequency response results for the isolated human passenger model are provided in Fig. 10 and are comparable to the results from Ref. 14. The testing of the isolated passenger model indicate the responses for human body parts to be very similar and higher than those for the seat components.

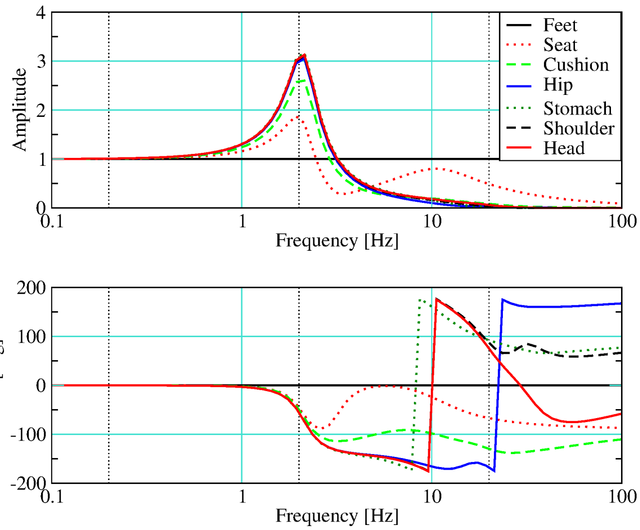

Figure 10: Frequency Response of Isolated Passenger Model

RIDE QUALITY ANALYSIS

There are different perspectives assessing the effects of operations in turbulent urban airwake, which is the focus of this study. In Tamer et al. (Ref. 14), the authors explored AAM/UAM vehicles operating in the turbulent urban airwake particularly for occupant ride comfort. Tamer et al. propose a modular and versatile simulation environment to approach comfort assessment involving a two-step method: first, a modular simulation framework generating overall vehicle models, including the aircraft and human body; second, results post-processing to incorporate human perception of vibration using ISO-2631 (Ref. 19). The approach was adopted for this study by development and implementation of a passenger biodynamic model in the AAM flight dynamics model and the assessment of the ride comfort for the operation in the turbulent airwake.

For this study, the ride quality assessment was performed for three operations of an AAM configuration in the urban airwake: (a) *hover-hold* at a rooftop landing location, (b) *approach to hover-hold* to the rooftop landing location, and (c) *straight and level flight* at different heights through an urban city canyon. The three scenarios were simulated using the FLIGHTLAB comprehensive model with the autopilot enabling flight path control. Pertinent information such as aircraft flight path, aircraft attitudes, rates, and accelerations, and passenger model accelerations were recorded during the simulation.

The ride quality analysis followed the procedure outlined in Tamer et al. (Ref. 14). The accelerations of the degrees of freedom of the biodynamic model representing the abdomen (hip), bowels (stomach), chest, and head were collected from the simulation of the flight dynamics. Frequency weighting per ISO-2631 standards was applied to incorporate human perception of vibration, as human sensitivity varies with excitation frequency. The passenger comfort was calculated in terms of the root mean square (RMS) of the weighted acceleration magnitudes over the flight time. Tamer et al. (Ref. 14) rates the ride comfort with reference to the averaged weighted magnitudes of the accelerations as: *comfortable* for $a_{rms} < 0.03g$, *low-comfort* for $0.03 \leq a_{rms} < 0.13g$, and *uncomfortable* beyond, $a_{rms} \geq 0.13g$.

The passenger model captures exclusively accelerations in the vertical axis with respect to the seat, i.e., along the passenger spine. The results presented in this publication therefore show the rating of the vertical human body accelerations. These initial ride comfort ratings explore additional effects on the ride quality estimate such as rigid/elastic fuselage model, steady wind/turbulent wind, and operational aspects for the three test scenarios. The goal is to explore the suitability of the proposed approach for estimating passenger ride comfort as a parameter used for AAM aircraft operational and safety considerations.

Hover Hold Simulation

Initial ride quality assessments were conducted in hover under steady and turbulent wind conditions using rigid- and elastic fuselage models. The hover hold is most straightforward for the autopilot model and was therefore suitable for the initial exploration of the ride quality prediction. A steady wind from the North, i.e., perfect head-on wind, was used for the hover-hold simulations. Turbulent wind data were constructed from a LBM simulation for a 4.5 m/s wind emanating perpendicular from the left of the building, see Fig. 8. After transients, the volumetric data were interrogated to form a volumetric table look-up with ≈0.4m separation distances. This table look-up was a precursor to the REM. The variation in the winds and turbulent content of the approach can be observed by the many different features in Fig. 8.

Figure 11 shows the simulation predictions for the passenger ride comfort for rigid-body and elastic fuselage models in steady and turbulent wind for the hover-hold maneuver. The ride quality predictions focus on the acceleration of the passenger abdomen (stomach) model. The response of the human passenger model was consistent with the tests of the isolated passenger model in Fig. 10 showing the largest response around 2 Hz. The ride comfort was rated as *comfortable* for all hover-hold test cases. The rigid-body model consistently produced slightly higher accelerations in the passenger model for hover in steady and turbulent wind. The accelerations for the model with rigid body in steady wind were lower than for the turbulent wind cases. However, the accelerations in steady and turbulent wind were in general small and well within the *comfortable* rating. The autopilot was capable of maintaining the hover position accurately for both steady and turbulent wind conditions.

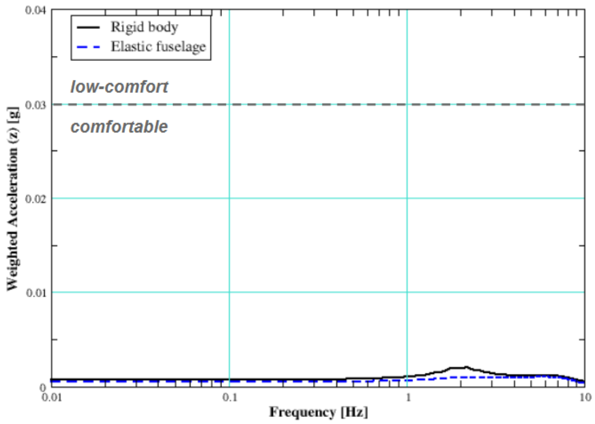

a) Steady Wind

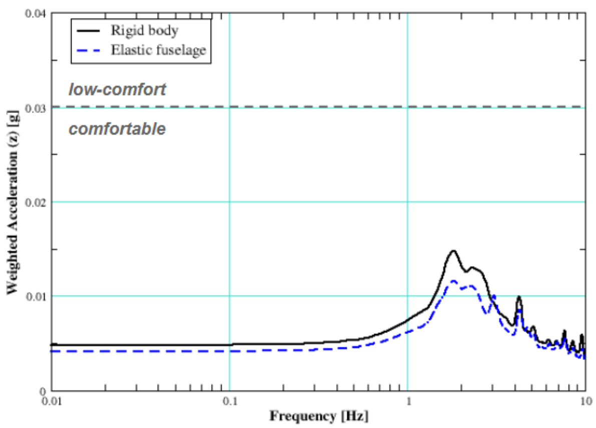

b) Turbulent Wind

Figure 11: *Hover-Hold Maneuver:* Ride Comfort Rating with Rigid-Body and Elastic Fuselage Models

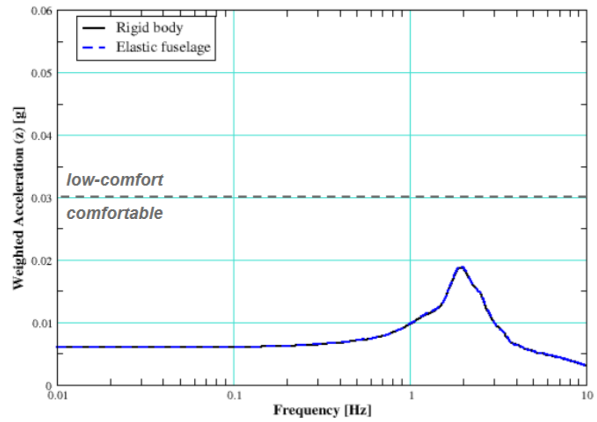

a) Steady Wind

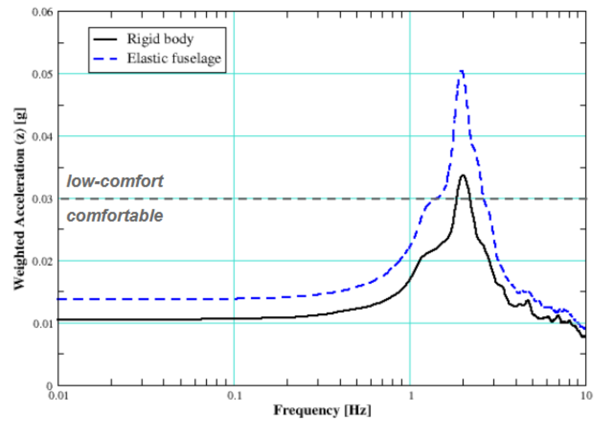

b) Turbulent Wind

Figure 12: *Approach-to-Hover Maneuver:* Ride Comfort Rating with Rigid-Body and Elastic Fuselage Models

Approach to Hover

In the second maneuver, the model is trimmed at approximately 8.75 m/s (17 kts) in forward level flight approaching the designated hover position. The turbulent wind data were the same as those applied in the Hover-Hold simulation. The autopilot controller reduces the forward speed and descends approximately 9.14 m (30 ft) to the hover location, see also the illustration in Fig. 8. The maneuver concludes with a short hover hold as performed in the previous section.

Figures 12a) and b) show ride quality predictions from the FLIGHTLAB simulation for the approach maneuver as performed with the rigid-body and elastic fuselage models and in steady and turbulent wind conditions, respectively. In the steady wind case without turbulence, both rigid and elastic fuselage models yielded similar *comfortable* ride quality ratings. However, for the turbulent wind conditions, the ride quality for elastic fuselage model indicates that the ride quality was degraded significantly, with portions of the flight falling within the *low-comfort* rating. In addition, even with the rigid fuselage model assumption, the flight extended slightly in the *low-comfort* region.

The turbulent wind components and the aircraft vertical aircraft accelerations in Figs. 13 and 14, respectively, provide the reason for the degraded ride quality for the approach to hover maneuver. The head-on wind, reflected in the wind x-component, indicated the largest variation in magnitude during the flight. There were also significant variations in the wind z-component, during the first 10 seconds of the test. The vertical wind component impacts the ride comfort model the most, since it is in the same axis as the passenger spinal chord.

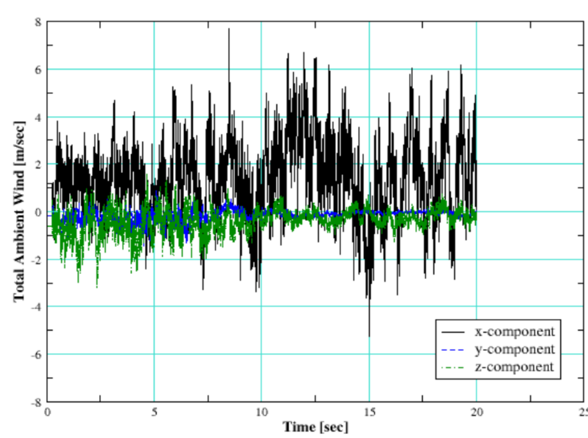

Figure 13: Wind Components

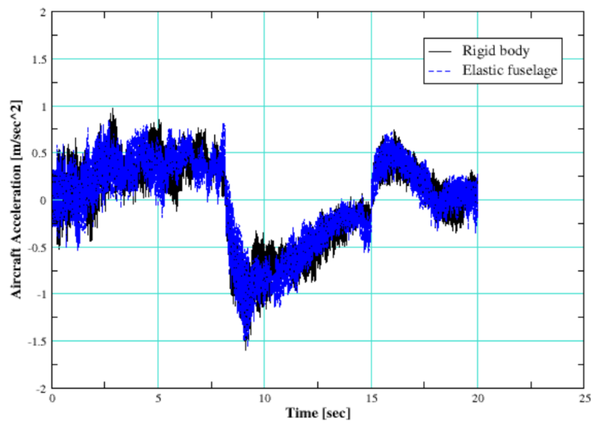

Figure 14: Aircraft Vertical Acceleration

Effect on Parts of Passenger Model

Since the previous ride comfort predictions focused on the acceleration of the passenger's abdomen, the ride comfort predictions for all passenger model components were assessed in the approach maneuver using the model with rigid fuselage model in the turbulent airwake.

Figure 15 deconstructs the weighted z-acceleration, i.e., in direction of the spinal chord, results of the power spectrum analysis for the individual parts of the passenger model in turbulent airwake during the approach-to-hover maneuver. The results indicate that the ride quality assessment provides similar results across the individual components of the human passenger model. The passenger seat and cushion show lower magnitude responses than the human passenger components, e.g., stomach, head, shoulders, etc. Furthermore, as the stomach (abdomen) showed similar ride comfort ratings as the other body parts modeled in the human passenger model, only this single component needs to be evaluated with this model.

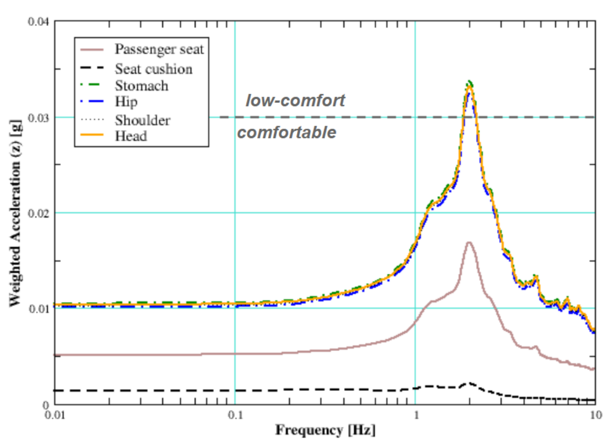

Figure 15: *Approach-to-Hover Maneuver:* Ride Comfort Ratings for Passenger Model Components in the Turbulent Airwake

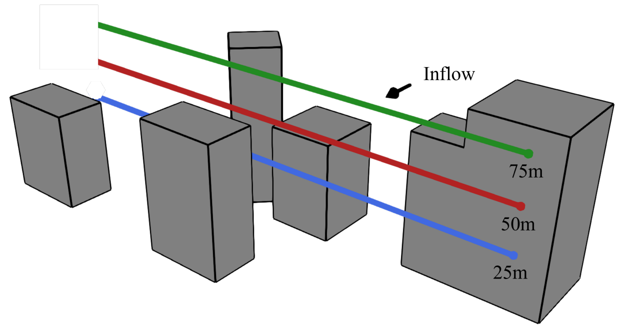

a) Orthogonal View of City Canyon

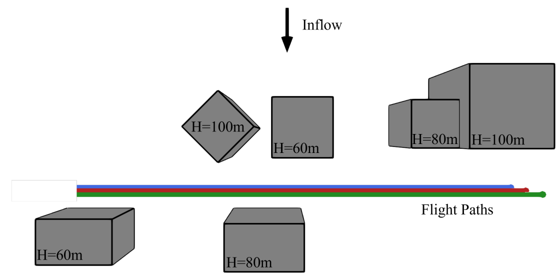

b) Top view with Annotated Building Heights

Figure 16: City Canyon for Level Flight Case. Flight occurred from left to right along the trajectories. Modified from Ref. 1

Level Flight in City Canyon

While terminal operations of hover and approach to landing are critical, the selection of the flight altitude during cruise can also influence ride quality. To assess this, straight and level flight in a city canyon at different heights above the ground, see Fig. 16, were assessed. This simulation applied a time history of the urban airwake x, y, z components from the externally generated airwake processes discussed previously, applied to all aerodynamic computation points of the flight dynamics model. The new approach of integrating externally computed airwake velocities is needed when a larger domain is covered in the flight simulation. The simulation was conducted exclusively with the flight dynamics model with elastic fuselage model.

For these simulations, the notional street was comprised of different size and orientation of buildings, as previously assessed in Waanders et al. (Ref. 1). The LBM (and REM) applied a nominal wind speed of 2.5 m/s (4.86 kts) at 50 m (164 ft) height with mild air turbulence. The resulting wind field, normalized by the 2.5 m/s (4.9 kts) wind speed (U_∞) along the flight path at the 50 m (164 ft) altitude is illustrated in Fig. 17. The large variations in the flight environment are obvious given the rapid color gradients. The rapid variations between buildings are of particular note with respect to ride quality, flight controls, and safety considerations.

The wind variation encountered by the vehicle along each flight altitude is presented in Fig. 18. The winds are similar to those from Ref. 1, but there are several differences, including

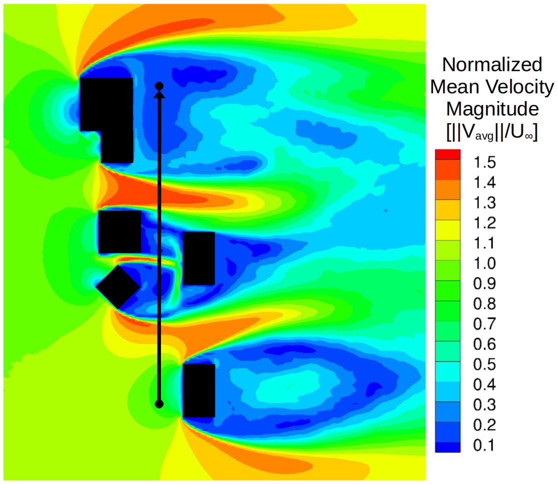

Figure 17: Turbulent wind field encountered during the 50 m (164 ft) flight path indicated in Fig. 16. Winds are normalized by the nominal wind speed of $U_\infty = 2.5$ m/s (4.9 kts).

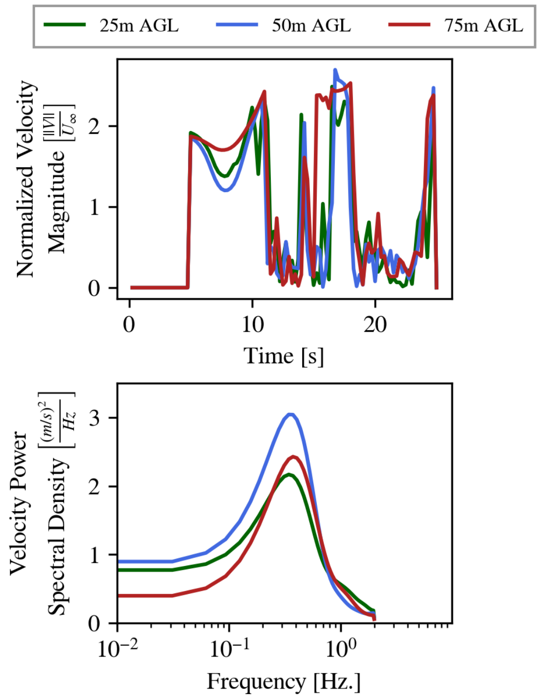

Figure 18: Unsteady velocity components and turbulence intensity encountered for the different flight altitudes indicated in Fig. 16.

the flight direction, which is opposite to that in Ref.1. The dataset applied here is based on a faster 20.6 m (40 kts) flight speed and interrogated at 0.25 seconds.

Figure 19 provides the ride comfort predictions for the flights at 25 (82), 50 (146), and 75 (246) m (ft) above the ground. As a baseline, a test was also conducted at 50 m without ambient wind for comparison. The ride comfort analysis of the abdomen acceleration of the passenger model resulted in: a marginally *low-comfort* rating at 25 m (82 ft) height, *uncomfortable* rating at 50 m (146 ft), and *low-comfort* rating at 75 m (246 ft) height above the ground, respectively. In comparison, the ride quality was rated *comfortable* for the flight at 50 m (146 ft) without ambient wind. The flight at 50 m (146 ft) height above the ground was at the approximate building height of the second building in Fig. 16a) which created an airwake making this height uncomfortable for the passenger. The best ride quality in the test was predicted for 75 m (246 ft).

These results can be compared with the unsteady conditions predicted by the external model and discussed in Waanders et al. (Ref. 1). The 50 m case was partially within the ABL roughness sublayer, see Fig. 1, with a mix of 60 (197) to 100 (328) m (ft) building heights and experienced the largest variation in wind velocity, as reported by Waanders et al. The vehicle experienced a local wind speed through the flight of up to almost three times the nominal mean wind. As the street was modeled in isolation, the roughness sublayer extends to the top of the buildings, so that the 75 m (246 ft) flight is along the edge of this turbulent domain, and experienced up to 1.5 times the wind variation. The 25 m (82 ft) AGL flight altitude was not evaluated in Waanders et al., but experiences some wind variation, exacerbated by its close proximity to the ground.

An interesting observation is that the peak of the power spectral density, multiplied by 10, observed both here in the LBM data (Fig. 18) and the REM data by Waanders et al. directly relates to the frequencies at which the ride quality exceeds the *comfortable* level. This implies that a potential correlation between the wind intensities and ride quality can be evaluated through examination of the wind field, but this hypothesis requires further evaluation.

The initial results are encouraging, demonstrating that the new approach of providing urban airwake data to the flight dynamics model was functional and resulted in reasonable and explainable responses from the passenger model. These results also indicate that an assumption of a steady wind, ignoring the influence of the urban canyon may not be acceptable.

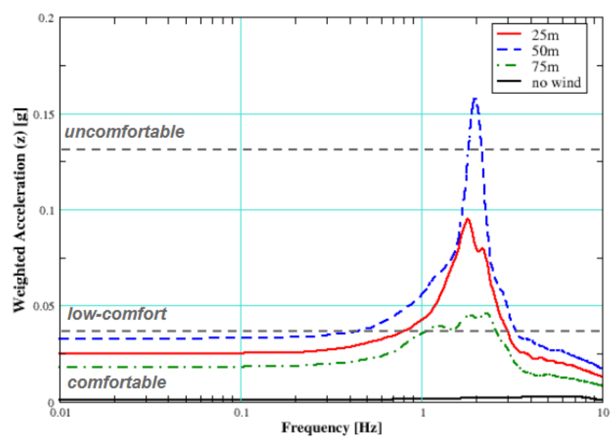

Figure 19: *Straight and Level Flight Through City Canyon Maneuver:* Passenger Ride Confort Rating

CONCLUSION AND NEXT STEPS

The simulation of AAM aircraft operations in turbulent airwake using comprehensive aircraft models has proven to provide important insight for developing safe and comfortable flight strategies in the urban environment. A realistic representation of the AAM aircraft benefits from the modeling of the pertinent features of the urban airwake, the elastic structure of the fuselage, and detailed coupling of flight control and electric propulsion systems. The proposed addition of a human passenger model allows the prediction of the ride comfort for human passengers.

The approach and hover-hold maneuvers used the established statistical airwake modeling templates previously developed and applied to the simulation of shipboard operations. However, in order to fly through larger domains of a city, a new approach was investigated which employs a dedicated software application calculating urban airwake velocity components at discrete locations, i.e., the aircraft aerodynamic computation points, and for every time step of the simulation. The proof of concept demonstrated in this paper provided encouraging results yielding ride comfort rating for a straight and level flight through a notional city canyon. The new approach will permit flight simulation within an urban airwake and a larger geographic area.

The ride quality analysis using simulation predictions from a human passenger model provides a qualitative assessment of the ride comport level. The ride quality assessment was sensitive to the modeling of elasticity of aircraft support structures. Therefore it is recommended to use elastic structures (e.g., elastic fuselage, wind, rotor mounts) to increase the quality of ride comfort predictions. The validation of ride comfort predictions with flight tests is desirable in the future.

A representative simulation of the aircraft flight dynamics is the foundation for the ride quality analysis. The urban airwake data used in this study captured the important features and characteristics of the urban air environment. The fight control system with autopilot for flight path following were coupled with a detailed electric propulsion system such that aircraft response to the urban turbulent airwake included the dynamics of the electric powertrain.

Next steps will complete the integration of the urban airwake wind component predictions in the comprehensive analysis model individually for all aerodynamic computation points and supporting real-time simulation. This will enable the expansion of simulations of AAM urban operations as piloted tests in engineering and training simulators, and provide an enhanced ability to improve safety of operations in these highly transient environments.

Additional evaluations are in progress to determine the numerical parameters (LBM mesh, REM interrogation points) so that the wind turbulent velocities and spectra are optimal for the assessment of ride quality and other metrics. This study will also integrated the improved reduced-order model developed by Seeyave et al. (Ref. 6). The wind data are currently linearly interpolated for the flight simulation model to minimize computation time; the influence of higher-order interpolation schemes on the wind data and ride quality are being evaluated.

Future concepts of AAM aircraft operation in the urban environment will exercise the proposed methodology to develop flight paths within a desired comfort level range and between city vertiports based on time of day, ambient wind magnitude and direction. An application to address changes in ambient environment and/or aircraft health status may also be explored with future analysis.

Author contact:
Jan Goericke: jan.goericke@flightlab.com
Marilyn J. Smith: ms55@gatech.edu
Dooyong Lee: dooyong.lee@flightlab.com

ACKNOWLEDGMENTS

Georgia Tech has been funded in part by the U.S. Government under Cooperative Agreement No. W911W6-21-2-0001, Mahendra Bhagwat is the technical monitor and the NASA University Leadership Initiative (ULI), Cooperative Agreement 80NSSC21M0113. Mia Siochi is the NASA technical monitor.

The views and conclusions contained in this document are those of the authors and should not be interpreted as representing the official policies of position, either expressed or implied, of the National Aeronautics and Space Administration (NASA) or the U.S. Government.

The authors would like to thank Georgia Tech graduate students Walter Chong, Aaron Crawford, Sheldon Salins, and Jeremy Seeyave who developed the REM methodology, and Duncan Waanders (co-advised by Dr. Juergen Rauleder) who provided LBM simulations. Special thanks also to Sheldon Salins for creating many of the wind field plots in this paper. Additional thank is extended to Felix Brenner from Gamma Technologies for the support on the electric propulsion system modeling and simulation.

REFERENCES

1. Waanders, D., Salins, S., Rauleder, J., and Smith, M. J., "A Real-Time Reduced-Order Model for the Atmospheric Boundary Layer Including Roughness Sublayer," Proceedings of the 81st Vertical Flight Society Annual Forum, VA Beach, VA, May 2025. DOI: 10.4050/F-0081-2025-325.

2. Stull, R., *Practical Meteorology: An Algebra-based Survey of Atmospheric Science -version 1.02b*, Dept. of Earth, Ocean & Atmospheric Sciences, University of British Columbia, `https://www.eoas.ubc.ca/books/Practical_Meteorology/`, 2017.

3. Oke, T. R., Mills, G., Christen, A., and Voogt, J. A., *Urban Climates*, Cambridge University Press, 2017.

4. Cantero, E., Sanz, J., Borbón, F., Paredes, D., and García, A., "On the Measurement of Stability Parameter over Complex Mountainous Terrain," *Wind Energy Science*, Vol. 7, (1), 2022, pp. 221–235. DOI: 10.5194/wes-7-221-2022.

5. Barlow, J. F., "Progress in Observing and Modelling the Urban Boundary Layer," *Urban Climate*, Vol. 10, ICUC8: The 8th International Conference on Urban Climate and the 10th Symposium on the Urban Environment, 2014, pp. 216–240. DOI: 10.1016/j.uclim.2014.03.011.

6. Seeyave, J., and Smith, M. J., "Spatio-Temporal Reduced-Order Modeling of Turbulent Flow at Very High Reynolds Number Using Machine Learning," Proceedings of the 51st European Rotorcraft Forum, Venice, Italy, September 9—12 2025.

7. Goericke, J., Brenner, F., and Lee, D., "Simulation and Analysis of Electric Motor Failure During eVtol Aircraft Operations in Turbulent Airwake," Proceedings of the 50th European Rotorcraft Forum, Marseille, France, September 10-12 2024.

8. Goericke, J., Muia, M., Habana, Z., and Batther, J., "Downwash/Outwash Investigation in Support of eVTOL Landing Operations," Proceedings of the VFS 6th Decennial Aeromechanics Specialists' Conference, Santa Clara, CA, February 6-8 2024.

9. Goericke, J., Brenner, F., Lee, D., and Habana, Z., "Investigation of eVTOL Operations in Turbulent Airwake Using Comprehensive Rotorcraft Analysis and Physics-Based Electric Propulsion System Models," Proceedings of the VFS 6th Decennial Aeromechanics Specialists' Conference, Santa Clara, CA, February 6-8 2024.

10. Simmons, B. M., Bunning, P., and Murphy, P., "Full-Envelope Aero-Propulsive Model Identification for Lift+Cruise Aircraft Using Computational Experiments," AIAA AVIATION 2021 Forum, Virtual, August 2–6 2021. DOI: 10.2514/6.2021-3170.

11. Silva, C., and Johnson, W., "VTOL Urban Air Mobility Concept Vehicles for Technology Development," Aviation Technology, Integration, and Operations Conference, Atlanta, GA, June 25–29 2018. DOI: 10.2514/6.2018-3847.

12. Peters, D., and He, C., "Finite State Induced Flow Models Part II: Three Dimensional Rotor Disk," Vol. 32 No.2, March-April 1995.

13. Gamma Technologies, "GT-SUITE Product," `https://www.gtisoft.com/gt-suite/`, 2025.

14. Tamer, A., Zanoni, A., and Masarati, P., "Comfort Assessment in Urban Air Mobility Vehicles," Proceedings of the 49th European Rotorcraft Forum, Bueckeburg, Germany, September 5-7 2023.

15. Wan, Y., and Schimmels, J. M., "Optimal Seat Suspension Design Based on Minimum Simulated Subjective Response," *Journal of Biomechanical Engineering*, Vol. 119, (4), 1997, pp. 409–416. DOI: 10.1115/1.2798287.

16. Choi, Y. T., and Wereley, N., "Biodynamic Response Mitigation to Shock Loads using Magnetorheological Helicopter Crew Seat Suspensions," *Journal of Aircraft*, Vol. 42, 2005, pp. 1288–1295. DOI: 10.2514/1.6839.

17. Federal Aviation Administration, "Advisory Circular: Aircraft Weight and Balance Control, AC 120-27F," `https://www.faa.gov/documentLibrary/media/Advisory_Circular/AC_120-27F.pdf`, Accessed: 07-22-2025, 2019.

18. U.S. Department Of Health And Human Services Centers for Disease Control and Prevention National Center for Health Statistics, "Anthropometric Reference Data for Children and Adults: United States, 2015–2018," Technical report, Series 3, Number 46, January 2021.

19. ISO/TC 108/SC 4, "Mechanical Vibration and Shock — Evaluation of Human Exposure to Whole-body Vibration, `https://www.iso.org/standard/50905.html`," Technical report, ISO-2631-1, International Organization for Standardization, July 2018.